R-99-05.1

Report on the Progress for the $\mu^+ \to e^+ + \gamma$ Experiment at PSI

Collaboration for $\mu^+ \to e^+ + \gamma$ Experiment at PSI

January 26th, 2001

The progress made in preparation for the $\mu^+ \to e^+ + \gamma$ experiment at PSI is reported. The status of the construction of the large prototype photon detector, the R&D with two prototypes of the drift chambers and the design of the COBRA spectrometer is described, followed by studies of the trigger system and plans for its implementation.

1 Photon detector large prototype

We are preparing a large prototype xenon detector to demonstrate the performance of the proposed xenon detector for high energy ($\approx$ 40 MeV) photons. With this prototype, we also intend to test various components of the detector, such as the photomultiplier tubes (PMTs), their support structure, the vacuum vessel, the regrigerator, the signal/HV feedthroughs, etc.

The construction of the vessel was completed at the end of last year (Figure 1). As an initial inspection, high pressure and cooling tests using gaseous nitrogen were carried out. The vessel was successfully filled with gaseous nitrogen up to 6 atm. at room temperature. Then, it was cooled down to below 165 K and the thermal inflow from the outside was estimated and found to be comparable to the design value. To evaluate the thermal inflow more precisely, more detailed studies will be done by filling the vessel with liquid nitrogen and monitoring the amount of evaporation. This result will be used to estimate the total heat load at liquid xenon temperature before the first test of xenon liquefaction in this vessel, which is planned in a few weeks.

We will use a pulse-tube refrigerator, developed at KEK, to keep the liquid xenon at a stable temperature and pressure after liquefying it by a liquid nitrogen cooling pipe. To measure its cooling power at 50–200 K the refrigerator was operated in a small test chamber. It proved to have a cooling power about 60 W at the operational temperature(165 K). It is thus powerful enough to compensate for the total heat load from the PMTs and from the outside.

The support structure of the PMTs is a miniature version of the final one (Figure 2(left)). The front side of the support is made of glass epoxy and plastic to reduce the amount of material which photons have to traverse. The feedthrough connectors for both signal and HV are those developed for the ATLAS liquid Ar calorimeter[1]. A picture of the signal feedthrough connector is shown in Figure 2(right). Many of the other components, such as the cables and connectors, are the same as those planned for the final detector. They will be intensively tested under the real conditions of detector operation.

2 R&D with the Tokyo drift chamber prototype

Tests have been performed with the first drift chamber prototype to study fundamental performances with the chamber cell structure described in the Proposal. Various gas mixtures, Ar/C_2H_6=50:50, He/C_2H_6=50:50, He/C_2H_6=60:40, and He/C_2H_6=70:30, were tried. We used a β-source of ^{90}Sr which emits 2.283 MeV electrons. The test setup is schematically shown in Figure 3.

Figure 1: Vessel for the large prototype.

Relative gains and drift velocities for each gas mixture were measured. In general, for gas mixtures with a higher percentage of He, the gains are higher (good for the vernier pad measurement) and the drift velocities are smaller (not good for high rate environment). An optimization of gas mixtures requires a detailed simulation study which incorporate these measured data.

By moving the source and collimator perpendicularly to the wire direction, the x-t relationships were obtained and the spatial resolutions were evaluated for each gas mixture. After subtracting the effects of the collimator and multiple scattering, resolutions of $100-150\ \mu m$ were generally obtained for helium based gas mixtures. This satisfies the requirement of $\leq 300\mu$m resolutions.

The spatial resolution along the wire by the charge division method using observed charges at both ends of wires was studied. It was found to be less than 2 cm at any point along the wires. This is good enough to select a particular vernier pattern which has a period of 6 cm.

The vernier pad measurements of hit positions along the wire use the ratios

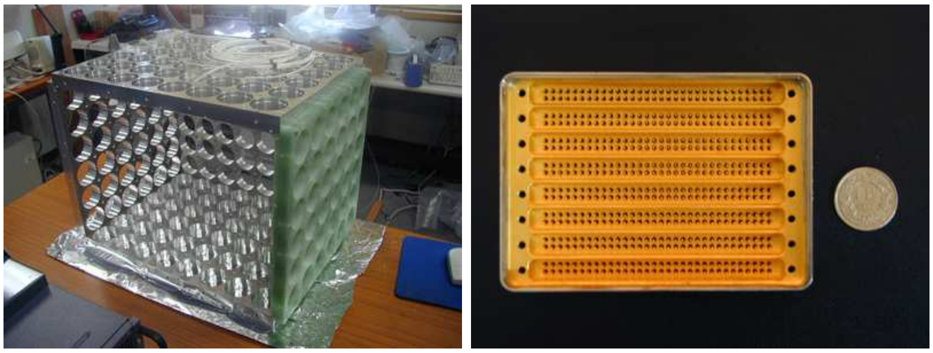

Figure 2: PMT holder (left) and signal feedthrough (right).

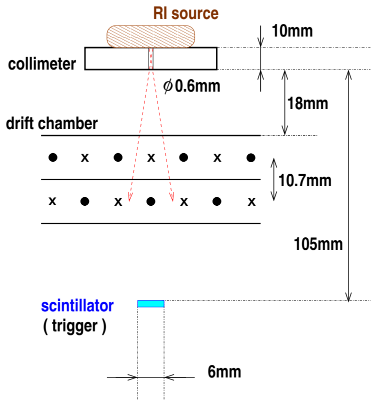

Figure 3: Setup for the drift chamber prototype test.

of charges induced on three pad (the right, center, and left pads):

$$R_{\mathrm{left}} = \frac{Q_{\mathrm{left}} - Q_{\mathrm{center}}}{Q_{\mathrm{left}} + Q_{\mathrm{center}}} \tag{1}$$

$$R_{\mathrm{right}} = \frac{Q_{\mathrm{right}} - Q_{\mathrm{center}}}{Q_{\mathrm{right}} + Q_{\mathrm{center}}} \tag{2}$$

Figure 4 shows an example of scatter plots for R_{left} and R_{right} for a gas mixture of He/C_2H_6(60:40) with a HV of 2000 volts applied on anode wires. A position along the diamond shape in the figure indicates the position along the anode wire. This distribution agrees well with that of the MC simulation.

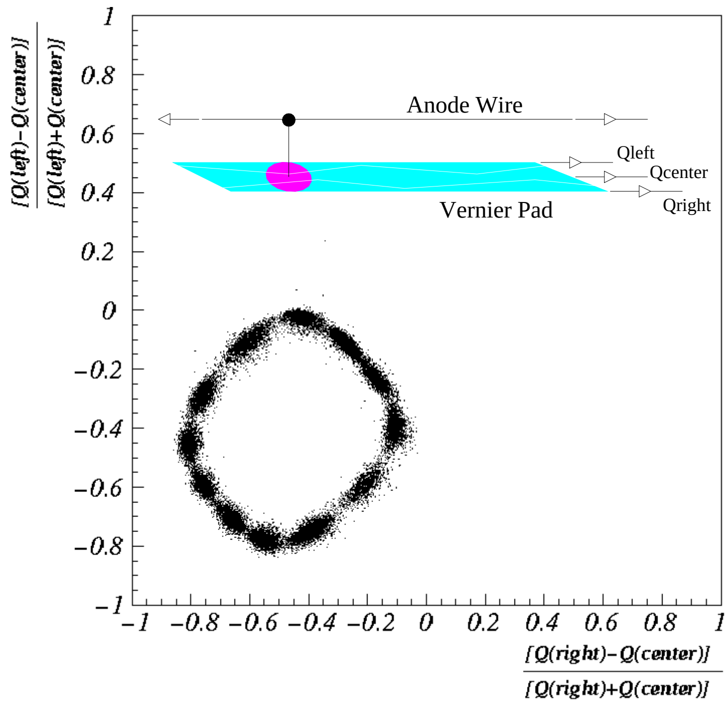

Figure 4: Correlation between R_{left} and R_{right} for various incident positions of the β rays along the anode wire.

A 400–800μm resolution was already attained in the preliminary measurement. More elaborate studies are under way to improve the resolution by optimizing the analysis method together with modifying the collimator and trigger system. An optimization of the vernier patterns, if necessary, will be considered later.

3 Work on the PSI Positron Tracker

Work on the Positron Tracker during the last six months, since the last Users Meeting BV31, has concentrated on the design and building of a miniature prototype drift chamber, as well as the preparations for and the testing of the chamber during a test-beam period in the πM1 area last October/November.

The chamber design, which was outlined previously [2], was governed by the need to test the chamber in a magnetic field comparable to that envisaged in the final experiment. This meant that the chamber was limited to a sensitive area of approximately (150x60) mm^2 in order to fit into the pole-gap of the dipole magnet, used as part of the momentum spectrometer in the test. The chamber consists of two planes, each of four or five, 20 μm sense-wires respectively and each spaced between 100 μm potential wires giving a drift-cell pitch of 5 mm. The two wire planes are staggered by half a cell and separated by an aluminized 15 μm cathode foil. The two outer cathode planes, consisting of an aluminized vernier pattern of three active strips per wire, have at present a thickness of 12.5 μm and were stretched as one continuous foil onto the outer Y-shaped chamber hood. This gives a total chamber gas-volume thickness of 14.4 mm. An exploded view of parts of the chamber is shown in Figure 5 below.

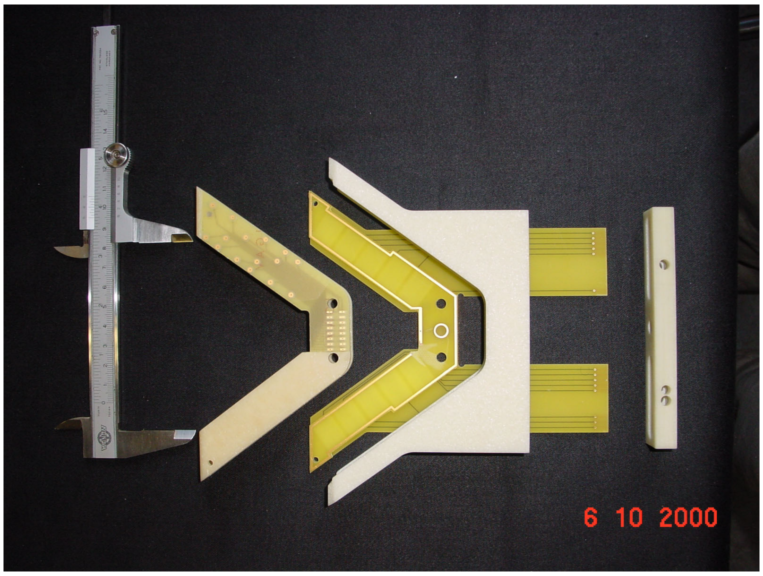

Figure 5: shows an exploded view of parts of the mini-prototype drift chamber used in the πM1 beam test. The main Steasalite frame (white), together with the one anode print and the central cathode plane (yellow), as well as one of the outer cathode planes with an active opening, shown by the callipers to be 80 mm are displayed.

The objectives of the test run were three-fold. Firstly, to measure the anode and cathode signal properties in order to optimize the design of the read-out electronics. Secondly, to measure the chamber characteristics as a function of such working conditions as, high voltage (gain) and magnetic field strength, in order to check the predictions from simulation, especially concerning the behaviour in a magnetic field. Finally, once the magnetic field characteristics of the standard gas (50%He : 50%Ethane) used in the test, confirms the simulations, then other candidate gas mixtures, to be tested in the laboratory without a magnetic field, maybe compared.

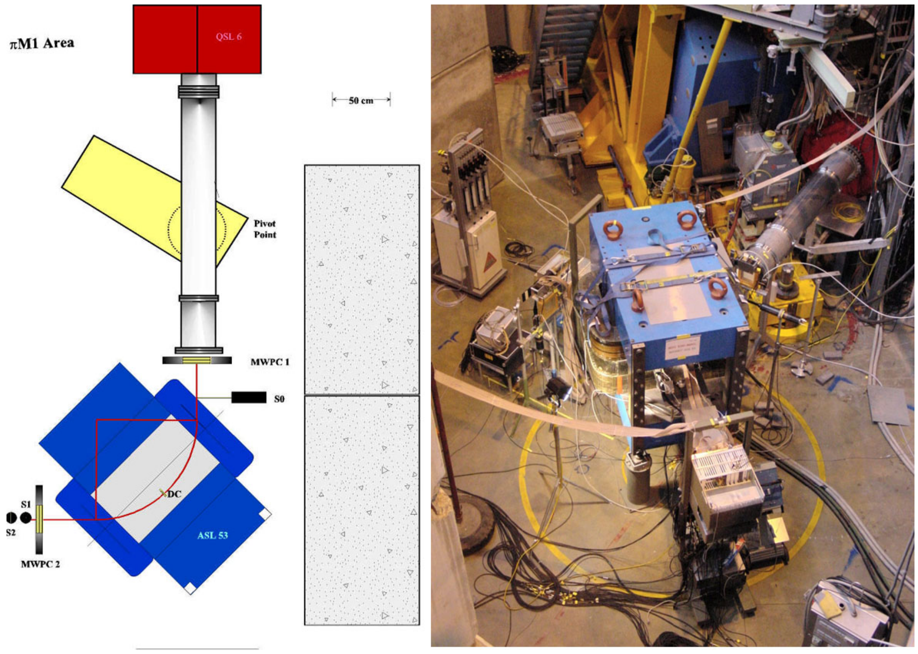

Figure 6: show respectively, the schematic view of the test setup and the actual used Bfield=on setup. The beam enters the area via the last quadrupole magnet QSL6 (red). Protons are removed by a CH2 -degrader placed in front of the first tracking chamber MWPC1. The beam trigger is defined by a scintillator telescope S0·S2 or S0·S1·S2, where S0 is a pill counter of 1mm diameter. MWPC2 is the final tracking chamber. The drift chamber (DC) is shown midway along the central trajectory with the magnet.

Figure 6 show respectively, a schematic view of the test beam setup and the actual setup used during the run. Two basic types of setup were used to collect data, one with Bfield=off, here MWPC2 and the trigger counter S2 were placed directly behind the drift chamber (DC), within the yoke of the C-shaped dipole magnet ASL53 and in direct line with the axis of the vacuum system. The Bfield=on setup, shown in the figure, allows a beam with small horizontal (20 mr) and vertical (10 mr) divergence to illuminate the full active region of the drift chamber. The trigger counters were positioned such that at the three momenta chosen, an optimal time-of-flight separation for all particle types (positrons, pions and muons), between Target M-S0 and S0-S2 was achieved. The three momenta of 158, 216 and 258 MeV/c, together with the 90deg bending angle of the magnet gave three reasonably spaced Bfield values (5.9, 8.2, 9.9 KG) with which to test the magnetic field dependency.

At present, the analysis of the data is in progress and first results confirm the functioning of the chamber, cf. Figure 7. However, the problem of noise experienced during the run is also apparent. This was predominantely due to the amplification electronics environment used. Also, there was a very limited time for testing the chamber prior to the run. Modification of the chamber readout prints is at present underway and will incorporate both the pre-amplification and post-amplification stages on the print in order to reduce noise. Once completed laboratory testing with the remaining candidate gas mixtures will continue.

4 The COBRA magnet

The high-strength aluminum stabilized superconductor, described in the previous report [2], is currently in production in industry (Hitachi Cable Ltd.), and will be ready for winding and assembling by the middle of this year.

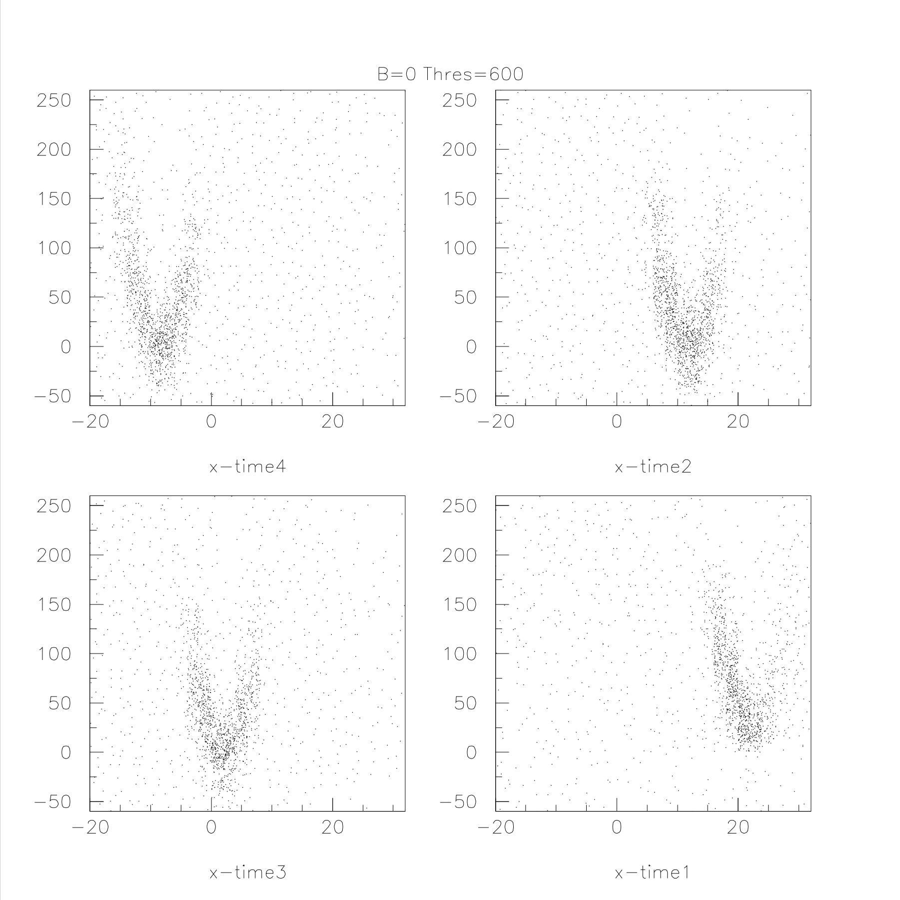

Figure 7: shows the drifttime-distance relationship for one plane of sense-wires. The horizontal axes show the x-coordinate in mm.(in the wire plane) vs. mean drifttime in ns.(average drifttime of both ends of the same wire).

In the meantime the mechanical design for the coil and the cryostat vessel have progressed greatly. In particular, we have investigated a possibility of using compensation coils to reduce the stray magnetic field in the vicinity of the photon detector.

There exists an optimized solution for the geometry of the compensation coils, which suppresses the stray field at the photon detector below ≈ 50 Gauss without any iron return yoke. All the essential features of the COBRA magnet, such as the constant bending radii and a fast sweeping of low energy positrons, are preserved in this design. It is currently being investigated whether the other detector components could fit into this design without compromising any fundamental performances.

5 Timing Counters

We have just received ten Bicron BC404 scintillator bars ($\sim 10\%$ of those necessary for the final counter) of dimensions 1 m $\times$ 5 cm $\times$ 1 cm and plan to use them to study the final configuration of the timing counter. Lightguides are currently being built to connect the scintillators to Hamamatsu 5924 PMTs (suitable to high magnetic fields) and to Philips XP2020 PMTs (which have a transit time spread comparable to the Hamamatsu type). The scintillators response will soon be tested over their full length by using cosmic ray muons. A technical design of the final timing counter set-up was recently started.

6 Trigger

Detailed simulation studies were performed in order to obtain an estimate of the final acquisition rate expected in the experiment. The background coming from the accidental coincidence of photons from the muon radiative decay $\mu^+ \to e^+\nu\overline{\nu}\gamma$ or from positron annihilation in flight and positrons from the normal muon decays was considered. A complete GEANT simulation of the proposed experimental set-up was used. We studied the selections based on the photon and positron kinematic variables which could be used in the trigger at various levels.

Photon energy and timing

The sum of the charge seen by the PMTs of the liquid xenon photon detector can be used by the trigger to obtain an estimate of the photon energy. By setting a threshold equivalent to a 45 MeV photon energy one achieves a $\sim$ 97% efficiency on the $\mu \to e\,\gamma$ signal while the fraction (per stopped muon) of background photons satisfying this selection criterion is $f_\gamma \simeq 2 \cdot 10^{-4}$. A trigger based only on this requirement would result in acquisition rate given by:

$$R_\gamma = R_\mu f_\gamma \Omega/4\pi \tag{3}$$

By using a stopping muon rate $R_\mu = 10^8 \mu/\mathrm{s}$ and a solid angle fraction of 10% we would obtain a 2 KHz photon trigger rate. We estimated that the rate in the timing counter due to Michel positrons is $R_{TC} \simeq 5 \times 10^6\,\mathrm{Hz}$. We can envisage a first level trigger given by the coincidence within $\Delta T = 10\,\mathrm{ns}$ of a photon in the liquid xenon detector and a positron in the timing counter. Such a first level trigger rate turns out therefore to be:

$$R_1 = 2R_\gamma R_{TC}\Delta T \approx 200\,\mathrm{Hz} \tag{4}$$

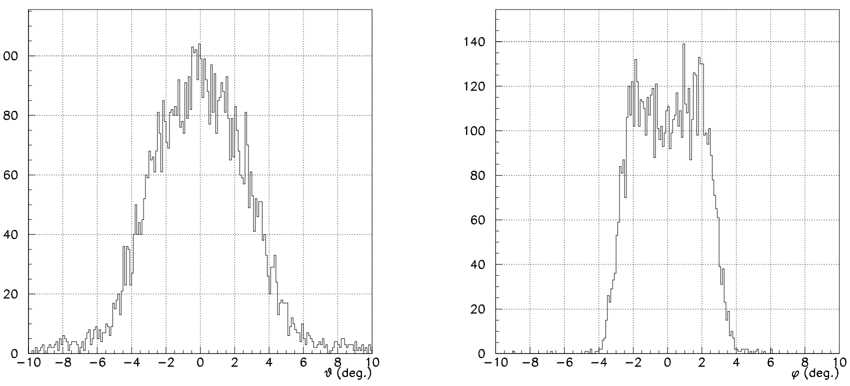

Figure 8: Photon direction determination by means of maximum light PMT.

6.1 Relative photon-positron direction

The position of the liquid xenon photon detector inner face PMT which observed the maximum light gives an estimate of the photon direction which is sufficient for trigger purposes. The determination of the photon direction obtained by connecting the maximum pulse height PMT with the center of the target is shown in fig.8 relatively to the true direction. A selection in ϕ corresponds, for $\mu \to e\gamma$ events, to an azimuthal selection of the timing counter scintillator bars hit by the positron, as can be seen from fig.9. We found that a 7.5 degree selection in ϕ corresponds to a spread over five scintillator bars for the positrons. The efficiency on the $\mu \to e\gamma$ signal of this selection is greater than 99.5%. For a flat background the corresponding rejection factor is $f_\phi \simeq 5$. The equivalent rejection factor in the zenith case is lower ($f_\theta \simeq 2$) due to the target bending along the beam axis. A trigger logic based on such an angular selection would result in a rate:

$$R_2 = \frac{R_1}{f_\phi f_\theta} \approx 20\,\mathrm{Hz} \tag{5}$$

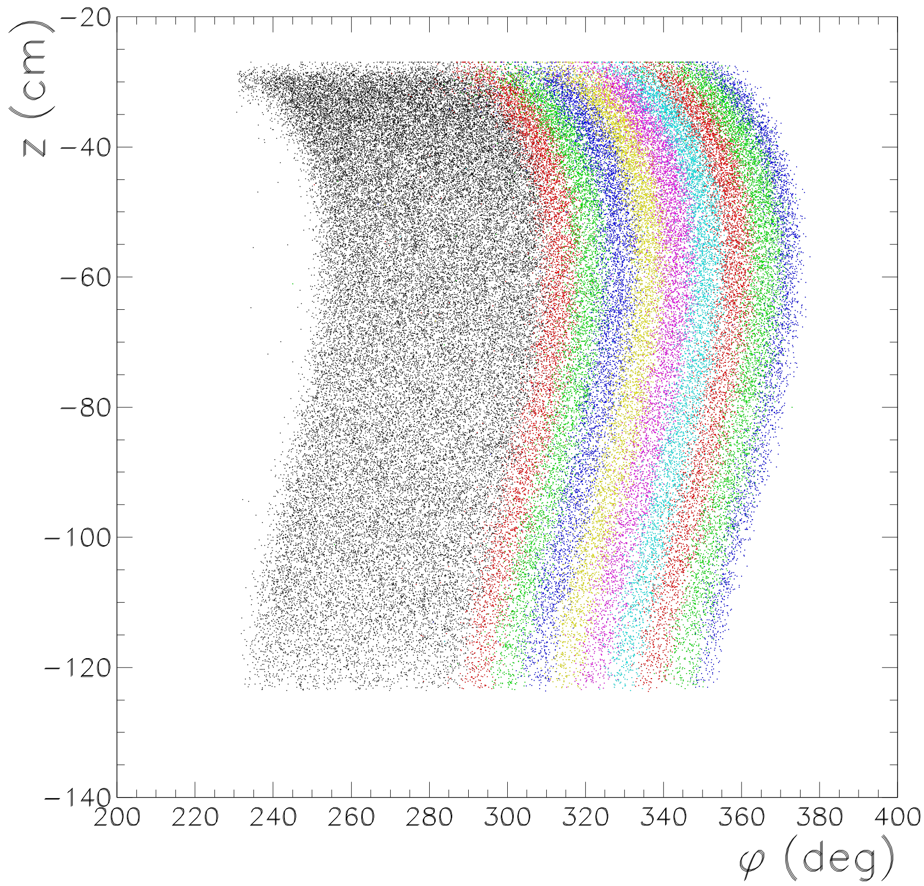

Figure 9: Hit patterns on Timing Counter for $\mu \to e\gamma$ positrons in the acceptance angular range. Different coloured bands correspond to 7.5 deg.-wide intervals in ϕ.

6.2 Positron energy

As illustrated in the proposal, the maximum radius (R_{DC}) reached by a positron in the drift chamber of the COBRA spectrometer is a measurement of its total momentum. For more than 99.5% of the positrons from $\mu \to e\gamma$ decays $R_{DC} > 26.5$ cm, which corresponds to leaving a signal in one of the last seven wires of a drift chamber of the COBRA spectrometer. We can envisage using the signals from these wires for an additional trigger level. However, a cut on the drift chambers radius does not correspond to a big rejection factor as can be seen from figure10 , where we show the momentum distribution of all the Michel positrons hitting the timing counter (continuous line) and those satisfying the previous condition on R_{DC}. The rejection factor that could be reached in this way is about 2.

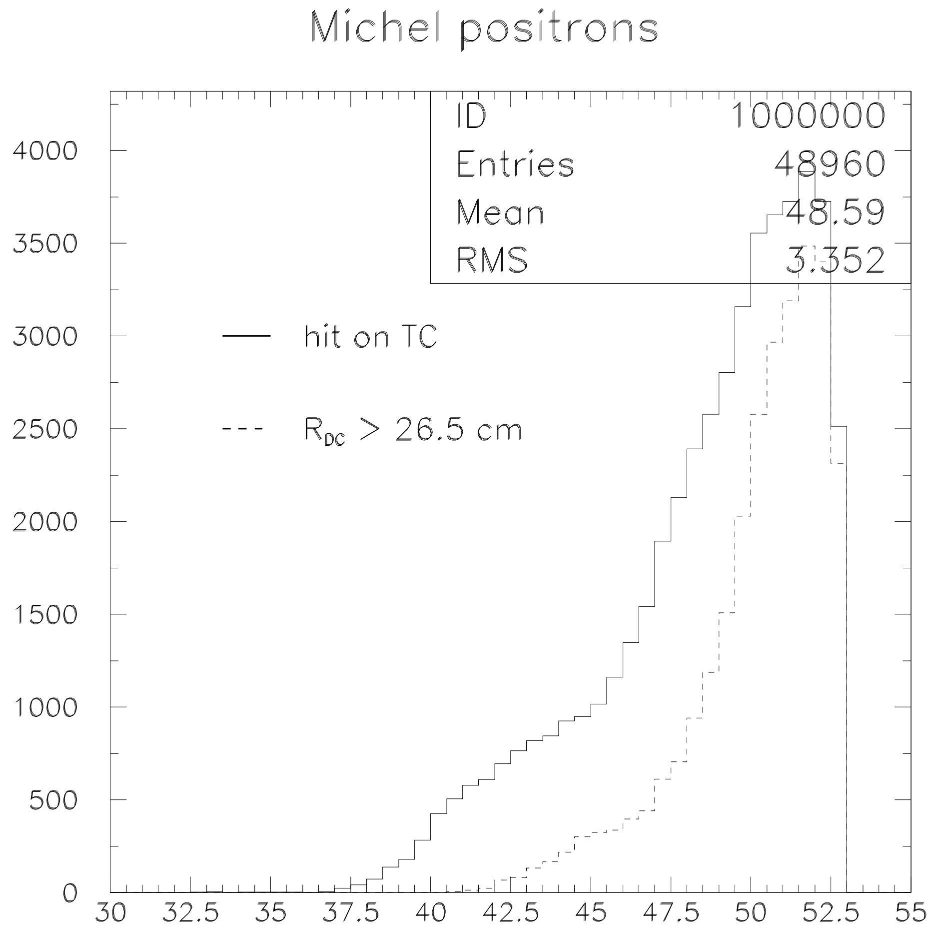

Figure 10: Momentum distribution of Michel positrons hitting the Timing Counter (solid line) and those with $R_{DC} > 26.5$ cm (dashed line).

6.3 Trigger Implementation

Simple selection criteria can reduce the acquisition rate due to the accidental background of our simulation to reasonable rates (less than 20 Hz). This rate gives us some margin in case of possible backgrounds not taken into account in the simulation. We are however studying further ways to keep other possible sources of backgorund under control. We are currently studying the schematics for accomplishing, in hardware, the selections discussed above, in the most flexible way by means of fast (100 MHz) signal digitization and the use of FPGAs.

First studies have shown that with today's high density FPGAs and fast flash ADCs it is possible to compute the overall charge sum of all PMTs from the LXe photon detector in about 200ns. Simultaneously, the PMT with the maximal charge and therefore the approximate position of the gamma interaction point can be found. This allows the correlation of the gamma and positron angles already at the first trigger level. A prototype VME board of the trigger is currently under development.

References

[1] ATLAS Liquid Argon Calorimeter Technical Design Report, CERN/LHCC/96-41, ATLAS TDR 2, December 15, 1996.

[2] Report on the Progress for the $\mu \rightarrow e\,\gamma$ Experiment at PSI, June 9, 2000.